Ultraviolet Broad Absorption Features and the Spectral Energy Distribution of the QSO PG 1351+64[1]

W. Zheng[2], G. A. Kriss[2,3], J. X. Wang[2,4], M. Brotherton[5], W. R. Oegerle[2,6]
W. P. Blair[2], A. F. Davidsen[2], R. F. Green[5], J. B. Hutchings[7], & M. E. Kaiser[2]

Received _____; accepted _____

Version 3.1, submitted to *Ap.J*

[1]Based on observations made for the Guaranteed Time Team by the NASA-CNES-CSA *FUSE* mission, operated by the Johns Hopkins University under NASA contract NAS5-32985, and observations with the NASA/ESA Hubble Space Telescope, obtained at the Space Telescope Science Institute, which is operated by the Association of Universities of Research in Astronomy, Inc., under NASA contract NAS5-26555.

[2]Center for Astrophysical Sciences, Department of Physics and Astronomy, The Johns Hopkins University, Baltimore, MD 21218-2686

[3]Space Telescope Science Institute, 3700 San Martin Drive, Baltimore, MD 21218

[4]Center for Astrophysics, University of Science and Technology of China, Hefei, Anhui, 230026, China

[5]Kitt Peak National Observatory, National Optical Astronomy Observatories, P.O. Box 26732, 950 North Cherry Ave., Tucson, AZ, 85726-6732

[6]Laboratory for Astronomy and Solar Physics, Code 681, Goddard Space Flight Center, Greenbelt, MD 20771

[7]Herzberg Institute of Astrophysics, National Research Council of Canada, Victoria, B. C. V8X 4M6, Canada

ABSTRACT

We present a moderate-resolution (~ 20 km s^{-1}) spectrum of the mini-broad-absorption-line QSO PG 1351+64 between 915–1180 Å, obtained with the Far Ultraviolet Spectroscopic Explorer (*FUSE*). Additional low-resolution spectra at longer wavelengths were also obtained with the Hubble Space Telescope (*HST*) and ground-based telescopes. Broad absorption is present on the blue wings of C III $\lambda977$, Lyβ, O VI $\lambda\lambda1032,1038$, Lyα, N V $\lambda\lambda1238,1242$, Si IV $\lambda\lambda1393,1402$, and C IV $\lambda\lambda1548,1450$. The absorption profile can be fitted with five components at velocities of ~ -780, -1049, -1629, -1833, and -3054 km s^{-1} with respect to the emission-line redshift of $z = 0.088$. All the absorption components cover a large fraction of the continuum source as well as the broad-line region. The O VI emission feature is very weak, and the O VI/Lyα flux ratio is 0.08, one of the lowest among low-redshift active galaxies and QSOs. The UV continuum shows a significant change in slope near 1050 Å in the restframe. The steeper continuum shortward of the Lyman limit extrapolates well to the observed weak X-ray flux level. The absorbers' properties are similar to those of high-redshift broad absorption-line QSOs. The derived total column density of the UV absorbers is on the order of 10^{21} cm^{-2}, unlikely to produce significant opacity above 1 keV in the X-ray. Unless there is a separate, high-ionization X-ray absorber, the QSO's weak X-ray flux may be intrinsic. The ionization level of the absorbing components is comparable to that anticipated in the broad-line region, therefore the absorbers may be related to broad-line clouds along the line of sight.

Subject headings: galaxies: active — galaxies: individual (PG 1351+64) — ultraviolet: galaxies

1. INTRODUCTION

Approximately 10% of QSOs at intermediate and high redshift show strong blueshifted absorption from ionized gas, which is being ejected, perhaps by radiation pressure from the central continuum source. Ejection velocities as large as 5×10^4 km s^{-1} lead to broad absorption troughs and a classic broad-absorption-line QSO spectrum (BALQSO, Turnshek 1988; Weymann 1995). Most absorption features are present below 1600 Å in the rest frame. A difficulty with studying this phenomenon in high-luminosity QSOs is the severe overlapping of the broad troughs that even mask the underlying continuum. The UV spectra obtained with *IUE* and *HST* open new windows, enabling one to study the absorption features at wavelengths well below 1200 Å (Turnshek et al. 1996; Korista et al. 1992). In low-luminosity QSOs, the velocity range is smaller, up to ~ 4000 km s^{-1}. Indeed, the absorption features in these objects may not be considered as "broad" while compared with that in the high-luminosity counterparts (Weymann et al. 1991), they are significantly broader and more displaced than the intrinsic absorption features in Seyfert-1 galaxies. Thus, these mini-BAL objects offer a possible extension of the BALQSO sample into the low-redshift domain (Malkan, Green & Hutchings 1987; Turnshek et al. 1995). The relatively low velocity structure makes separating and identifying individual components in the absorption trough much easier. At low redshifts, there is less confusion from intervening lines.

The nature and location of the absorbing gas is not known. Since the cores of emission lines are sometimes completely absorbed, the absorbers must lie at least somewhat beyond the broad emission-line region. If the absorption covering fraction with respect to the nuclear continuum is near 100%, the BAL phenomenon would be unique to a special group of objects, which would be physically different from all other "normal" active galactic nuclei (AGN). Conversely, if the covering factor is small, it is possible that most QSOs contain such outflows. They are then only recognized as BALQSOs if our line of sight to the central continuum source happens to pass through the outflow (Weymann 1995; Murray & Chiang 1995). However, Becker et al. (2000) found that the distribution of BAL in their radio-selected sample is not consistent with a simple unified model that BALQSO are seen edge-on.

The broad-band energy distribution of BALQSOs has special characteristics. It has been known that BALQSOs are not powerful radio sources (Stocke, et al. 1992). Becker et al. (2001) found that the number of high-ionization BALQSOs drops significantly for QSOs with a radio-loudness parameter $R^* > 100$. Richards (2001) found a small excess of narrow absorption toward radio-loud QSOs and toward lobe-dominant QSOs. There is also a small excess of high-velocity C IV absorbers in radio-quiet QSOs as compared to radio-loud quasars. BALQSOs are weak in the X-ray band (Green et al. 1995; Gallagher et al. 1999; Brandt, Laor, & Wills 2000). The average power-law index α_{ox} ($f_\nu \propto \nu^{-\alpha}$) derived between

2500 Å and 2 keV is $\gtrsim 1.9$, as compared to 1.5 for other low-redshift QSOs (Yuan et al. 1998). Thus the X-ray level in BALQSOs is about one order of magnitude weaker than average (Green & Mathur 1996). The nature of such distinctions is poorly understood, and further studies may reveal special physical conditions that are intrinsically associated with the BAL phenomenon.

PG 1351+64 (z=0.088) is one of the few mini-BAL QSOs identified at low redshifts. Its *IUE* spectrum (Brosch & Gondhalekar 1984) displays significant broad absorption in Lyα and C IV. A tentative analysis of the *HST* Faint Object Spectrograph (*FOS*) spectra identifies at least three absorption components in the blue wings of C IV, Lyα, and other UV lines (Granados et al. 1993). This object exhibits a weak X-ray flux around 1 keV, with a power-law index of $\alpha_{ox} = 1.9$ (Tananbaum et al. 1986).

In this paper we present the far-UV spectrum of PG 1351+64 obtained with the Far Ultraviolet Spectroscopic Explorer (*FUSE*), along with the *FOS* and *STIS* spectra obtained with the *HST*, and optical spectra. The moderate O VI absorption and the lack of other significant broad low-ionization absorption features suggest a moderate ionization state in the absorber. The O VI emission is exceptionally weak, consistent with the prediction of photoionization models with a soft UV-X-ray continuum shape.

2. DATA

FUSE is an instrument dedicated to high-resolution spectroscopy in the far-ultraviolet spectral region, and it was launched on 1999 June 24. It features multiple mirrors, Rowland-circle spectrographs and two-dimensional detectors. The LiF-coated optics yield a wavelength coverage of $\sim 979 - 1187$ Å, and the SiC-coated optics cover $\sim 905 - 1104$ Å. For a full description of *FUSE*, its mission, and its in-flight performance, see Moos et al. (2000), and Sahnow et al. (2000).

The *FUSE* observations of PG 1351+64 were carried out between 2000 January 18 and 20, for a total exposure time of 70 ks. The observations were made with the $30'' \times 30''$ low-resolution aperture. Because of a slight mis-alignment between the optical systems, not all detector channels record signals that are of photometric quality. Some data in this observation suffer from unexpected abnormalities that have not been fully understood during the calibration process.

We first combined all the raw data to produce four images in different detector segments. Two spectra were extracted from the two-dimensional data on each segment. These eight extracted spectra were dark subtracted and corrected for the background stray light. Flux

and wavelength calibrations were carried out with the standard *FUSE* calibration pipeline, which assumes a constant value of dark counts. To obtain the best estimate of the zero flux level, we used the Galactic absorption feature C II 1036 Å, which appears in all four channels, as a calibrator: i.e., the very bottom of this absorption feature represents a completely absorbed region, therefore a zero flux level. We estimate that the flux scale is accurate to $\sim 10\%$, and that wavelengths are accurate to ~ 15 km s^{-1}.

We have studied all the sections of data from every channel, and only chosen those that are free of abnormalities. The data near the edge of the detector segments often show an abnormal rise in flux and therefore cannot be used. The spectra were binned by 5 pixels, to preserve the full spectral resolution of ~ 20 km s^{-1} for this observation. The spectrum shown in Fig. 1 is produced by binning the data by 20 pixels (0.12 Å) to show the overall appearance of the spectrum. The S/N level around 1080 Å is considerably poorer, because of gaps in the wavelength coverage from the various detectors.

As part of a joint *FUSE-HST* project, two complementary *HST STIS* snapshot observations were made on 1999 October 28. The exposure was 600 s for the observation with the G140L grating, and 300 s with G230L. Due to the short exposures and low source flux, the *STIS* spectra do not have an adequate S/N level for fitting line profiles. We therefore retrieved archival *FOS* spectra of PG 1351+64, which has a spectral resolution of $\lambda/\Delta\lambda \sim 1300$. The *HST* spectra between 1150 and 3300 Å of PG 1351+64 were obtained on 1991 September 5. The exposure time for the G130H, G190H, and G270H spectra were, respectively, 3200, 3000, and 1400 s. The flux levels of the *STIS* and *FOS* spectra match each other to within 10%.

We used the *IRAF* task specfit (Kriss 1994) to fit the *FUSE* and *FOS* data. The wavelength scale of *FOS* data was slightly shifted with respect to the Galactic absorption features in the spectra. The O VI emission features (see Fig. 1) were fitted with four Gaussian profiles: a narrow doublet and a broad doublet. For the Lyβ, Lyα, N V, C IV and Mg II emission lines, a narrow component and a broad one were assumed. Other emission lines were fitted with one Gaussian profile. We fixed the widths and velocities of the two components of Lyβ to that of Lyα, and linked N V with that of C IV (see Table 1). The absorption lines were treated as Gaussians in optical depth, and they were allowed to partially cover the emission components. Note that the covering factor is along the line of sight, not the overall value around the source as described in section 1. The wavelengths of the O VI doublets were linked at the ratio of their laboratory values, and their relative optical depths were fixed at a 2:1 ratio. We used five (A, B, C, D & E) components to fit the O VI absorption doublets, and fixed the widths and covering factors of the other absorption lines to that of O VI, linking the velocities to that of O VI (a small linear shift in wavelength is permitted

for lines from different detectors). The only exception is component E: its covering factor cannot be well constrained by O VI as its component is too weak. We derived the covering factor for component E from the C IV absorption features in the *FOS* data. Component E of Lyβ is apparently narrower than its counterparts in other lines, so we set it free to vary. Because of different data quality, the *FUSE* data and *FOS* spectra were fitted separated, with only several linked parameters as discussed above. Galactic Lyman-line absorption was modeled with the best estimated hydrogen column density and a varying Doppler parameter. An extinction correction of $E_{B-V} = 0.05$ was applied using the estimated Galactic hydrogen column density of 2.5×10^{20} cm^{-2} (Lockman & Savage 1995), and the correction curve of Cardelli, Clayton & Mathis (1989) with $R_V = 3.1$. The spectrum between 1100 and 1140 Å is plotted in Fig. 2 to show details of the O VI features and the goodness of the fit.

We obtained optical spectroscopy of PG 1351+640 using the GoldCam spectrograph mounted on the 2.1-m telescope at Kitt Peak National Observatory. GoldCam currently uses a Ford 1000 × 3000 pixel CCD detector, with a useful area of 400 × ~2400 pixels in which a long slit spectrum is focused and can be well calibrated. The blue spectrum (~3200-5900 Å useful coverage) was obtained through a wide slit (6″) and using a 500 l mm^{-1} grating blazed at 5500 Å (resolution ~9 Å) for 300 s on 2000, February 25 (UT). Weather conditions were generally good on that night, but variable seeing (up to 3″) and some thin clouds resulted in non-photometric spectra. The red spectrum (~5800-9800 Å useful coverage) was formed by combining narrow slit (1″.5) observations from two nights, both taken using a 400 l mm^{-1} grating blazed at 8000 Å (resolution ~12 Å) and an OG 550 order-blocking filter: the exposure time on February 25 was 400 s, and on February 26 900 s. The spectra were weighted by their counts in the combination. Standard stars were used to divide out atmospheric absorption, but the air masses were not well matched and the division is imperfect. The red spectrum flux level was scaled to match that of the blue, which in turn was scaled up by a factor of 1.67 to match that from the *HST* spectrum (although the signal-to-noise ratio in the region of overlap was only 3, making the absolute scaling factor uncertain). We employed standard data reduction techniques within the NOAO IRAF package.

Archival *ROSAT* Position-Sensitive Proportional Counter (PSPC) data were retrieved from the High Energy Astrophysics Science Archive Research Center (HEASARC) at NASA Goddard Space Flight Center. We use the data taken in 1993 October, with an exposure time of 3776 s. The *ROSAT* spectrum was fitted using *xspec* (Arnaud 1996) with a single power law and Galactic absorption. The fits generated satisfactory results ($\chi_r^2 < 0.8$) for most spectra. Our results yield a photon power index $\Gamma = 2.69 \pm 0.2$ for a fixed column density of 2.6×10^{20} cm^{-2}, in good agreement with Rush & Malkan (1996). Dual power laws produced only minimal improvements, and therefore they were not used in the final results.

Fig. 4 shows the unfolded spectrum with error bars that reflect the combined contributions from propagation errors, known flux variations, and the uncertainties of the Galactic column density (10^{19} cm^{-2}).

3. Discussion

3.1. Emission Lines

Fig. 5 displays the profiles of seven major UV emission lines and the Hα line. The fitted parameters for the UV lines are listed in Table 1. We will focus our discussion on the features longward of 1050 Å because of their higher signal-to noise ratios.

The most significant finding is the weak O VI emission: its intensity measured on the red wing is only about 28% of that of C IV or 8% of that of Lyα, which is among the lowest in all AGN and QSOs. The O VI/Lyα ratio in the QSO composite spectrum of Zheng et al. (1997) is only 0.19 ± 0.02. Fig. 2 shows the full profile of the O VI emission. The broad O VI component appears to be even weaker: the O VI/Lyα ratio between the broad components is only ~ 0.02.

There is an excess of flux on the blue wings of the Balmer lines, as shown in Fig. 5. Such a bump is also seen in another published spectrum (Corbin & Boroson 1996). We fitted each of the Balmer lines with Gaussian profiles, which are a poor match. The fitted profiles are displayed with dashed curves. The excess blue flux may be due to electron scattering or from the outflowing matter that is part of the broad-line region.

The *FUSE* spectra reveal two emission lines at $\sim$ 1160 and 1168 Å, and we tentatively identify them as S IV $\lambda\lambda$1062,1073. Such a feature has been noticed, but without a firm identification, by Laor et al. (1994, 1995), and Hamann et al. (1998). It is also noted as absorption in the spectrum of NGC 4151 (Kriss et al. 1995). The wavelength of 1168Å coincides with the second-order feature of the terrestrial airglow line He I, but the feature is much broader than any airglow line. At lower spectral resolution, such features may have been found as part of the red wing of the O VI profile in the HST QSO composite spectrum (Zheng et al. 1997).

The fitted He II emission component is very broad, and it includes blended features such as an unidentified component at $\sim$ 1620Å (Laor, et al. 1994, 1995).

3.2. Absorption Lines

In Table 2 we list the measurements of major absorption lines, named as components A, B, C, D, and E. The absorption present in the *FUSE* data is also obviously present in the *FOS* spectrum. For components A, B, C, D, the line velocities and widths derived from the *FUSE* data can also fit the *FOS* data well, but the derived H I column densities are quite different (higher than *FOS*). This may well be due to the lower resolution of *FOS* data, and saturation in the Lyα profile. The presence of Mg II absorption is highly uncertain as no individual components can be seen.

To determine physical conditions in the absorption components, we used CLOUDY (Ferland et al. 1998) to calculate models. In a grid of photoionization calculations, we vary the ionization parameter U from 0.001 to 30. We used a broken power-law ionizing continuum with indices of $\alpha = 1.9$ and 0.7 between 13.6 eV-2 keV and 2-10 keV, respectively, and assumed a hydrogen density of 10^{10} cm^{-3} and solar abundances. However, variations of these parameters do not affect the results significantly.

Because the *FOS* and *FUSE* data were not obtained simultaneously, and because of the higher spectral resolution of the *FUSE* data, we will focus on *FUSE* data. For components A, B, C, D, we detected obvious O VI and Lyβ absorption. From our grid of photoionization models, we determine the total column density and the ionization parameter U based on the observed relative H I and O VI column densities. With no other constraints, this method can lead to double-valued results for the ionization parameter and column density since the ratio of O VI to H I will rise to a peak and then decline when U increases. However, we note that the presence of clear C III absorption in components A, C, D restricts the solutions to the lower ionization parameter in these cases, thus yielding small ionization parameters ($U < 0.3$), and a total column density $< 10^{20}$ cm^{-2}. Even if we choose a model with a high ionization parameter, the total column density is on the order of 10^{21} cm^{-2}, insufficient to cause significant X-ray obscuration. Table 3 lists the column densities, derived ionization parameters for the five absorbers.

3.3. Continuum

The continuum in the *FUSE* data is fitted with a power law of $\alpha = 3.92 \pm 0.05$. The fitted power-law index for the *FOS* data is $\alpha = 1.69 \pm 0.01$, which is considerably flatter than that for the *FUSE* data. This suggests a change in the continuum shape around 1050 Å in the rest frame, consistent with but even more dramatic than that found in typical QSOs (Zheng et al. 1997; Kriss et al. 2000a). To make sure that this is not an extinction effect, we

carried out a continuum fit to the combined *FUSE-FOS* spectrum in the wavelength region below 2000 Å. A simple power law with variable extinction yields a significantly poorer fit (best fitted value $E_{B-V} = 0.06$) than a broken power law with a fixed Galactic extinction ($E_{B-V} = 0.05$). Therefore, the break in the continuum is intrinsic.

Zheng et al. (1997) suggested that Compton scattering in a hot corona above the disk modifies the exponential turnover of the thermal disk spectrum into a power law in the EUV band. In the case of PG 1351+64, a corona with lower temperature than average may produce the steep EUV/soft X-ray power law. The extrapolation of the soft *FUSE* continuum leads to the weak X-ray level that has been observed. Rush & Malkan (1996) observed a weak X-ray flux level and a steep X-ray spectrum (photon index $\Gamma \sim 2.6$) in their *ROSAT* observations pf PG 1351+64, which is consistent with an extrapolation of our *FUSE* spectrum. The continuum between the UV and soft X-ray bands can be approximated with a power law with $\alpha_{ox} = 1.9$ (Tananbaum et al. 1986). The short baseline in the sub-Lyα region does not allow us to assess whether the far-UV and the soft X-ray continuum can be approximated with a single power law. However, to a first approximation, such a soft EUV continuum may be common among low-luminosity AGN with broad absorption. Another similar QSO, PG1411+44, shows an even softer X-ray to UV flux ratio with $\alpha_{ox} = 2.1$ (Laor et al. 1997). Green & Mathur (1996) suggested that a torus of total column density of $N >> 10^{22}$ cm^{-2} may produce a significant depression of the soft X-ray flux. But in PG 1351+64, the weak soft-X-ray flux is consistent with the far-UV continuum shape. Furthermore, we do not see signs for obscuring material of such high column density in the UV or in the optical data.

Green et al. (1995) analyzed the data of all BALQSOs in the ROSAT All-Sky Survey and found that they are either highly absorbed or underluminous in the soft X-ray bandpass. They suggest that the weak X-ray level may be due to heavy obscuration. Brandt, Laor & Wills (2000) find a significant correlation between the X-ray weakness in AGN and the strength of the C IV absorption and suggest that absorption may be the cause of the weak X-ray flux. In the case of PG 1351+64, the photoionization calculations and the lack of an intrinsic Lyman edge suggest that the total nucleon column density is less than 10^{22} cm^{-2}. This is not sufficient to obscure the X-ray continuum, and the soft UV-X-ray continuum is probably intrinsic.

3.4. Comparison with Other AGN and QSOs

It has been suggested that radio-quiet QSOs with weak [O III] and strong Fe II emission spectra form a class of QSOs that has a high probability of exhibiting BAL in their spectra (Boroson & Meyers 1992; Turnshek et al. 1997). In the two BALQSOs 0759+65 (Turnshek

et al. 1997) and 1700+51 (Turnshek et al. 1995), significant Mg II absorption and continuum extinction are also present. In this regard, PG 1351+64 does not fit this category: its [O III] intensity is about the same as the Hβ line, the intensity of its optical Fe II emission is only moderately weak, and no Mg II absorption is obvious in PG 1351+64 (Fig. 5).

In terms of UV spectral features, PG 1351+64 bears a strong resemblance to PG1411+44. Their nearly identical redshifts make the two spectra remarkably alike. There are significant spectral differences however: (1) PG 1411+44 has weaker O [III] emission, by a factor of about four, with respect to the Hβ; and strong optical Fe II features are present; and (3) PG 1411+44's soft-X-ray flux level is significantly lower (by a factor of three or more); and (4) its He II λ1640 emission is exceptionally strong, suggesting a harder ionizing continuum in the EUV band. Laor et al. (1997) found that the X-ray spectrum of PG1411+44 above 2 keV exhibits a significant upturn, suggesting strong obscuration in the soft X-ray band. Since PG 1351+64 does not present such characteristics, it may belong to a different group despite the similarity of its Lyα and C IV absorption to that of PG1411+44.

The ionization structure of the absorbers in PG 1351+64 seems to be comparable to the UV absorption components seen in many Seyfert-1s (e.g., NGC 4151: Kriss et al. 1995; NGC 3516: Kriss et al. 1996a, b; Mrk 509: Kriss et al. 2000b) and with those observed in many high-redshift objects (Turnshek 1988; Korista et al. 1992), albeit at a smaller ejection velocity. Most of these objects do not show broad Mg II absorption lines, and the C IV, N V, and O VI column densities are at a comparable level to PG 1351+64. More work is needed, however, to understand the difference in their X-ray properties.

4. Summary

PG 1351+64 is one of the handful of mini-BALQSOs. The *FUSE* spectrum allows us to identify and measure five kinematically distinct components. Model calculations with multiple species suggest column densities on the order of a few $\times 10^{21}$ cm^{-2} for the absorbing clouds. These clouds would not produce significant absorption in the soft X-ray band. Therefore the object's weak X-ray flux may be intrinsic unless there is significant absorption from more highly ionized material. Additional evidence in support of an intrinsically weak X-ray flux exists from the very weak O VI emission, as well as the significant downturn of the far-UV continuum shortward of 1050 Å.

Table 1. UV Emission Lines in PG 1351+64.

Line	Wavelength (Å)	Flux[a] $(10^{-14}\,\mathrm{ergs\,s^{-1}\,cm^{-2}})$	FWHM[b] $(\mathrm{km\,s^{-1}})$	Velocity[b,c] $(\mathrm{km\,s^{-1}})$	Comment
C III	977	11.9 ± 2.9	2538 ± 1417	344 ± 552	
Lyβ narrow	1026	5.1 ± 0.4	1367	225	
Lyβ broad		9.4 ± 0.1	7764	-1412	
O VI narrow	1034	25.6 ± 0.5	2660 ± 83	-444 ± 143	
O VI broad		6.4 ± 1.0	8597 ± 995	-407 ± 114	
S IV	1062	5.5 ± 0.2	1416 ± 33	617 ± 26	
S IV	1073	6.7 ± 0.6	1368 ± 103	606 ± 112	airglow?
Lyα narrow	1216	123 ± 2	1367 ± 21	225 ± 10	
Lyα broad		330 ± 5	7764 ± 201	-1412 ± 41	
N V narrow	1240	17 ± 2	2491 ± 16	129 ± 23	
N V broad		116 ± 4	8198 ± 222	795 ± 49	
C II	1335	3.2 ± 0.4	1045 ± 183	200 ± 61	
Si IV + O IV]	1400	62 ± 2	4486 ± 390	-762 ± 64	
C IV narrow	1549	57 ± 1	2491 ± 16	129 ± 23	
C IV broad		74 ± 1	8198 ± 222	795 ± 49	
He II	1640	23 ± 8	18757 ± 3709	4420 ± 1428	blend
O III]	1664	11 ± 2	9312 ± 1299	-1813 ± 325	
Al III	1857	12 ± 1	4021 ± 1123	1010 ± 607	
Si III]	1892	17 ± 2	3406 ± 995	358 ± 393	
C III]	1909	29 ± 3	2853 ± 724	551 ± 321	
Mg II narrow	2798	7 ± 4	1367 ± 207	195 ± 120	
Mg II broad		57 ± 8	7407 ± 591	3 ± 137	Fe II?

[a]Corrected for $E_{B-V} = 0.05$.

[b]Values without errors are fixed.

[c]With respect to the systemic velocity of 26,400 $\mathrm{km\,s^{-1}}$ (Malkan et al. 1987).

Table 2. UV Absorption Lines in PG 1351+64

Line	Wavelength (Å)	Component	Column density (10^{14}cm^{-2})	FWHM (km s^{-1})	Velocity[a] (km s^{-1})	Covering factor[b]
C III	977.02	A	1.81 ± 0.64	198 ± 15	-780 ± 23	0.71 ± 0.02
		B	0.44 ± 0.28	250 ± 10	-1049 ± 8	0.60 ± 0.04
		C	0.37 ± 0.12	135 ± 8	-1629 ± 10	0.80 ± 0.04
		D	1.33 ± 0.62	134 ± 16	-1833 ± 8	0.75 ± 0.02
		E	2.99 ± 0.56	613 ± 60	-3054 ± 125	0.87
Lyβ	1025.72	A	11.7 ± 1.9	198 ± 15	-780 ± 23	0.71 ± 0.02
		B	6.14 ± 1.90	250 ± 10	-1049 ± 8	0.60 ± 0.04
		C	4.29 ± 2.54	135 ± 8	-1629 ± 10	0.80 ± 0.04
		D	0.93 ± 0.36	134 ± 16	-1833 ± 8	0.75 ± 0.02
		E	1.89 ± 0.42	65 ± 8	-3054 ± 125	0.87
O VI	1031.93,1037.62	A	26.2 ± 2.8	198 ± 15	-780 ± 23	0.71 ± 0.02
		B	41.5 ± 8.7	250 ± 10	-1049 ± 8	0.60 ± 0.04
		C	7.06 ± 2.02	135 ± 8	-1629 ± 10	0.80 ± 0.04
		D	13.9 ± 8.9	134 ± 16	-1833 ± 8	0.75 ± 0.02
		E	0.96 ± 0.59	613 ± 60	-3054 ± 125	0.87
Lyα	1215.67	A	3.32 ± 0.17	407 ± 14	-779 ± 17	0.71
		B	0.48 ± 0.20	189 ± 25	-1479 ± 10	0.60
		C	0.11 ± 0.08	114 ± 8	-1633 ± 7	0.80
		D	0.72 ± 0.33	234 ± 14	-1964 ± 11	0.75
		E	1.26 ± 0.15	587 ± 17	-3132 ± 10	0.87 ± 0.02
N V	1238.81,1242.80	A	8.90 ± 0.41	497 ± 14	-869 ± 17	0.71
		B	1.06 ± 0.25	189 ± 25	-1479 ± 10	0.60
		C	1.71 ± 0.36	114 ± 8	-1633 ± 7	0.80
		D	1.14 ± 0.24	234 ± 14	-1964 ± 11	0.75
		E	6.17 ± 0.69	587 ± 17	-3132 ± 10	0.87 ± 0.02
Si IV	1393.76,1402.77	A	0.80 ± 0.24	497 ± 14	-869 ± 17	0.71
		B	0.19 ± 0.23	189 ± 25	-1479 ± 10	0.60
		C	0.08 ± 0.06	114 ± 8	-1633 ± 7	0.80
		D	0.25 ± 0.30	234 ± 14	-1964 ± 11	0.75
		E	0.39 ± 0.30	587 ± 17	-3132 ± 10	0.87 ± 0.02
C IV	1548.19,1550.77	A	5.65 ± 0.16	407 ± 14	-869 ± 17	0.71
		B	1.02 ± 0.17	189 ± 25	-1569 ± 10	0.60
		C	1.43 ± 0.16	114 ± 8	-1723 ± 7	0.80
		D	1.02 ± 0.17	234 ± 14	-2054 ± 11	0.75
		E	3.64 ± 0.81	587 ± 17	-3222 ± 10	0.87 ± 0.02

[a]With respect to the systemic velocity of 26,400 km s^{-1}.

[b]Values without errors are fixed.

Table 3. Properties of the Absorbers in PG 1351+64.

Species	Component				
	A	B	C	D	E
Column density(cm^{-2})					
HI	1.1×10^{15}	6.1×10^{14}	4.2×10^{14}	8.2×10^{13}	1.3×10^{14}
CIII	1.8×10^{14}	4.3×10^{13}	3.7×10^{14}	1.3×10^{14}	3.0×10^{14}
OVI	2.62×10^{15}	4.2×10^{15}	7.1×10^{14}	1.4×10^{15}	1.0×10^{14}
$\log U$	-1.19	-1.00	-1.23	-0.74	-1.23
N_{total} (cm^{-2})	2.1×10^{19}	1.8×10^{19}	7.3×10^{18}	4.4×10^{18}	9.6×10^{17}
Covering factor	0.71	0.60	0.80	0.75	0.87

REFERENCES

Arnaud, K. A. 1996, in ASP Conf. Series 101, Astronomical Data Analysis Software and Systems V, , ed. G. Jacoby & J. Barnes (San Francisco: ASP), 17

Becker, R. H., White, R. L., Gregg, M. D., Brotherton, M. S., Laurent-Muehleisen, S. A.; & Arav, N. 2000, ApJ, 538, 72

Becker, R. H., et al. 2001, astro-ph/0104279

Boroson, T. A., & Meyers, K. A. 1992, 397, 442

Brandt, W. N., Laor, A., & Wills, B. J. 2000, ApJ, 528, 637

Brosch, N., & Gondhalekar, P. M. 1984, A&A, 140, L43

Cardelli, J., Clayton, G., & Mathis, J. 1989, ApJ, 345, 245

Corbin, M. R., & Boroson, T. A. 1996, ApJS, 107, 69

Ferland, G. J., Korista, K. T., Verner, D. A., Ferguson, J. W., Kingdon, J. B., & Verner, E. M. 1998, PASP, 110, 761

Gallagher, S. C., Brandt, W. N., Sambruna, R. M., Mathur, S.; Yamasaki, N. 1999, ApJ, 519, 549

George, I. M., Turner, T. J., Mushotzky, R.,

Granados, A., Sachs, E., Shull, J. M., & Stocke, J. T. 1993, in The Evolution of Galaxies and Their Environment, ed. D. J. Hollenbach, H. A. Thronson, & J. M. Shull (Moffett Field Calif.: NASA Ames Research Center), 115

Green, P. J., & Mathur, S. 1996, ApJ, 462, 637

Green, P. J., et al. 1995, ApJ, 450, 51

Hamann, F., Cohen, R. D., Shields, J. C., Burbidge, E. M., Junkkarinen, V., Crenshaw, D. M. 1998, ApJ, 496, 761

Korista, K. T., et al. 1992, ApJ, 401, 529

Kriss, G. A. 1994, in Astronomical Data Analysis Software and Systems III, A.S.P. Conf. Series, V. 61, ed. D. R. Crabtree, R. J. Hanisch & J. Barnes (San Francisco: Astronomical Society of the Pacific), 437

Kriss, G. A., Davidsen, A. F., Zheng, W., Kruk, J. W., & Espey, B. R. 1995, ApJ, 454, L7

Kriss, G. A., Espey, B. R., Krolik, J. H., Tsvetanov, Z., Zheng, W., & Davidsen, A. F. 1996a, ApJ, 467, 622

Kriss, G. A., et al. 1996b, ApJ, 467, 629

Kriss, G. A., Davidsen, A. F., Zheng, W., & Lee, G. 2000a, ApJ, 527, 683

Kriss, G. A., et al. 2000b, ApJ, 538, L17

Laor, A., Fiore, F., Elvis, M., Wilkes, B. J., & McDowell, J. C. 1997, ApJ, 477, 93

Laor, A., Bahcall, J. N., Januzzi, B. T., Schneider, D. P., Green, R. F., & Hartig, G. F. 1994, ApJ, 420, 110

Laor, A., Bahcall, J. N., Januzzi, B. T., Schneider, D. P., & Green, R. F. 1995, ApJS, 99, 1

Lockman, F. J., & Savage, B. D. 1995, ApJS, 97, 1

Malkan, M. A., Green, R. F., & Hutchings, J. B. 1987, ApJ, 322, 729

Moos, H. W., et al. 2000, ApJ, 538, L1

Murray, N., & Chiang, J. 1995, ApJ, 454, L105

Richards, G. T. 2001, ApJS, 133, 53

Rush, B., & Malkan, M. A. 1996, ApJ, 456, 466

Sahnow, D., et al. 2000, ApJ, 538, L7

Stocke, J. T., Morris, S. L., Weymann, R. J., Foltz, C. B. 1992, ApJ, 396, 487

Tananbaum, H., Avni, Y., Green, R. F., Schmidt, M., & Zamorani, G. 1986, ApJ, 305, 57

Turnshek, D. A. 1988, in QSO Absorption Lines: Probing the Universe, ed. J. C. Blades, D. A. Turnshek, & C. A. Norman (Cambridge: Cambridge Univ. Press), 17

Turnshek, D. A., Foltz, C. B., Weymann, R. J., Lupie, O. L., McMahon, R. G., & Peterson, B. M. 1985, ApJ, 294, L1

Turnshek, D. A., Kopko, M., Jr., Monier, E., Noll, D., Espey, B. R., & Weymann, R. J. 1996, ApJ, 463, 110

Turnshek, D. A., Monier, E., Sirola, C. J., & Espey, B. R. 1997, ApJ, 476, 40

Weymann, R. 1995, in QSO Absorption Lines, ed. G. Meylan (Berlin: Springer), 213

Weymann, R. J., Morris, S. L., Foltz, C. B., Hewett, P. C. 1991, ApJ, 373, 23

Wills, B. J., Brandt, W. N., & Laor, A. 1999, ApJ, 520, L91

Yuan, W., Brinkmann, W., Siebert, J., & Voges, W. 1998, A&A, 330, 108

Zheng, W., Kriss, G. A., Telfer, R. C., Grimes, J. P., & Davidsen, A. F. 1997, ApJ, 475, 469

Figure Captions

Fig. 1.— *FUSE* spectrum of PG 1351+64, binned to $\sim$ 0.12 Å (20 pixels). 1σ errors are displayed as dotted lines. The data between 1070 and 1100 Å are not as reliable because they lie in a gap of several detector segments.

Fig. 2.— Best fit to the O VI emission and absorption features. The data are binned by five pixels. The residuals are displayed at the bottom. The centroid wavelengths of the fitted O VI and Lyβ absorption components are marked with their assigned names.

Fig. 3.— Combined *STIS* and *FUSE* Spectrum of PG1351+64. The *STIS* data below 1750 Å are not used due to abnormalities, and the *FOS* G190H spectrum is overplotted to fit the wavelength gap. Galactic absorption features are marked with a "G".

Fig. 4.— Broad-band energy distribution of PG 1351+64. Corrections are made for a hydrogen column density of 2.5×10^{20} cm^{-2} and extinction of $E_{B-V} = 0.05$.

Fig. 5.— Major absorption features and their absorption counterparts. The vertical dashed lines mark the position of five absorption components, and the arrow signs in panel a, c, f and g represent the other doublet components. The zero level approximately represents that of the fitted continuum.
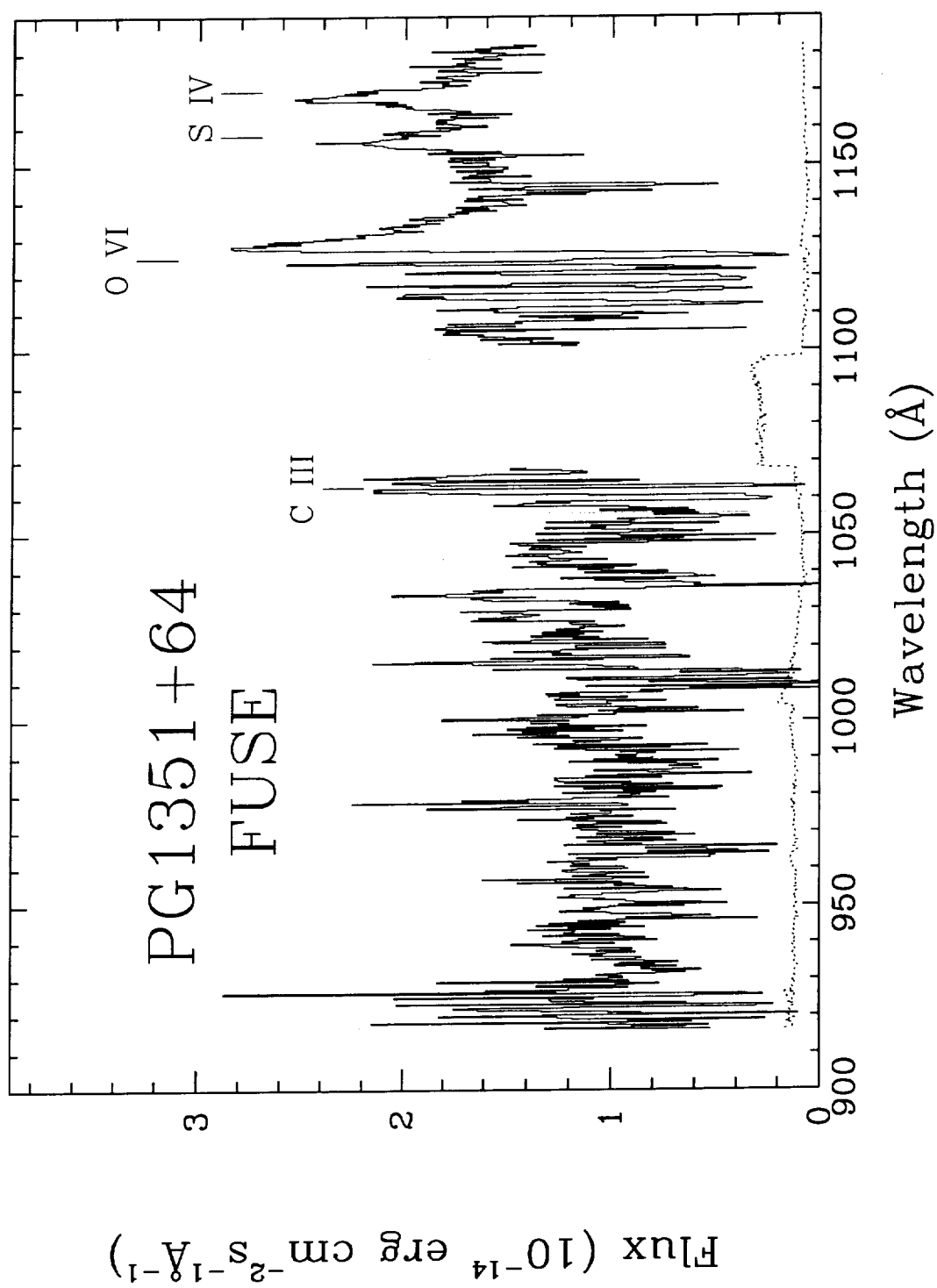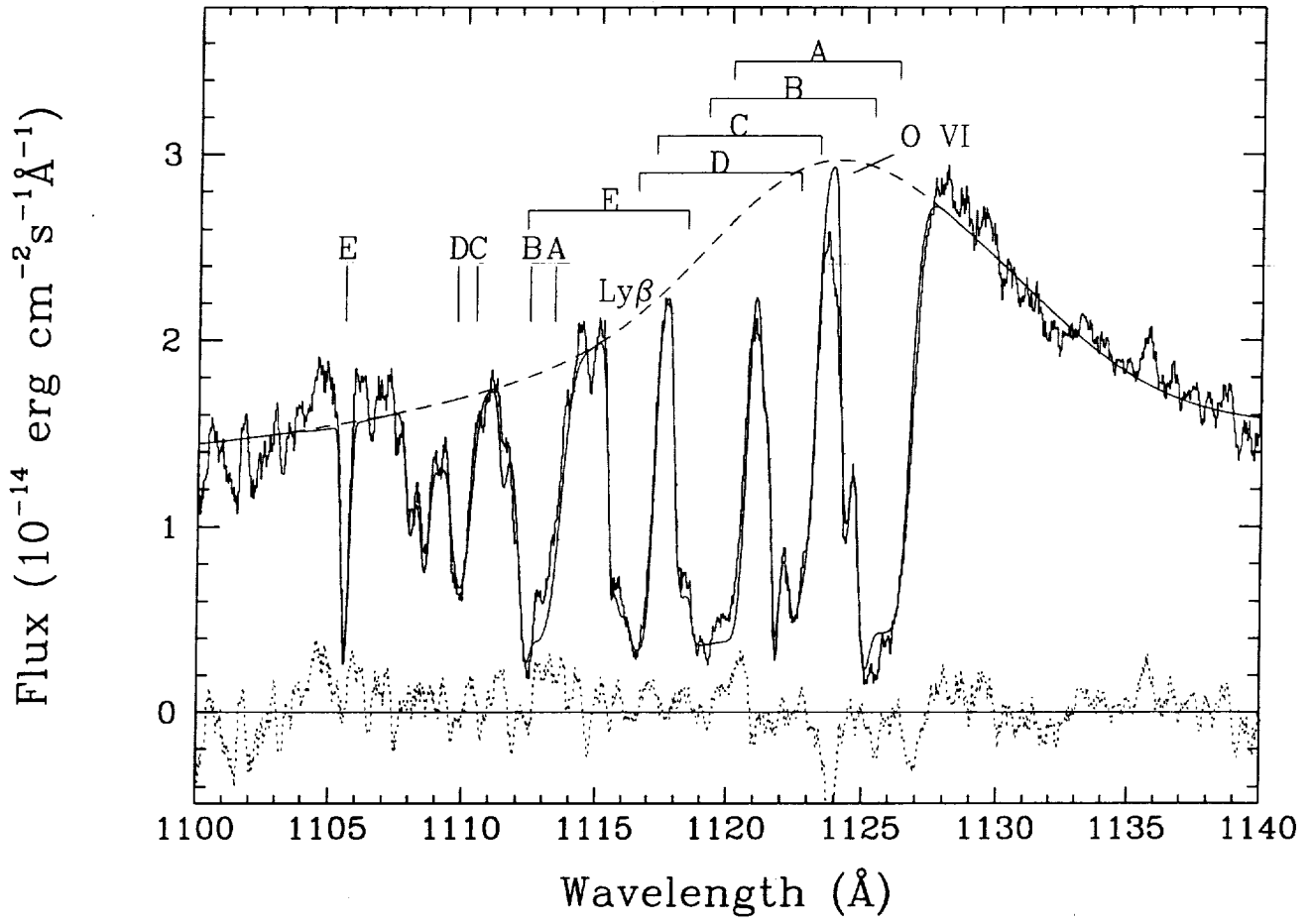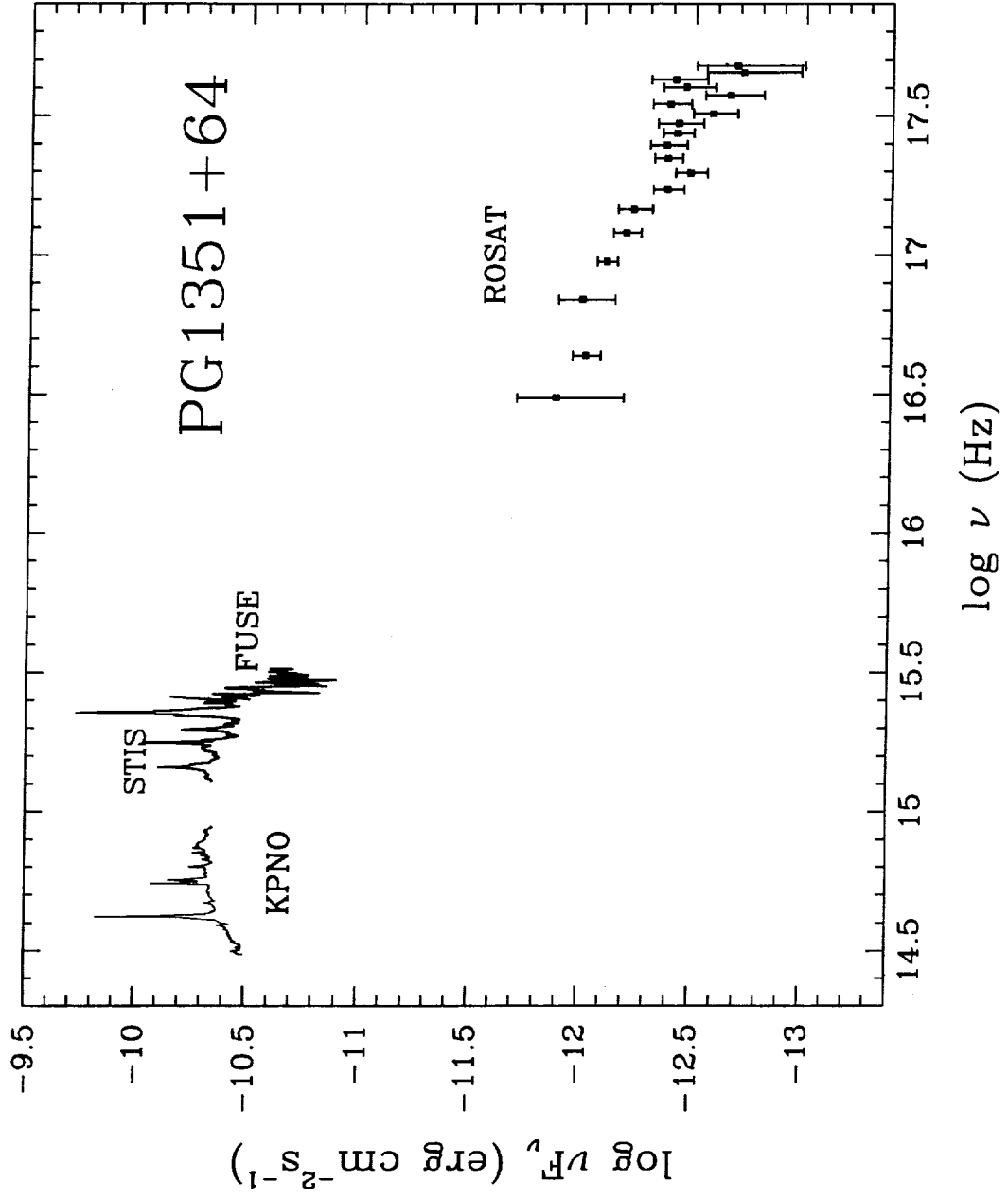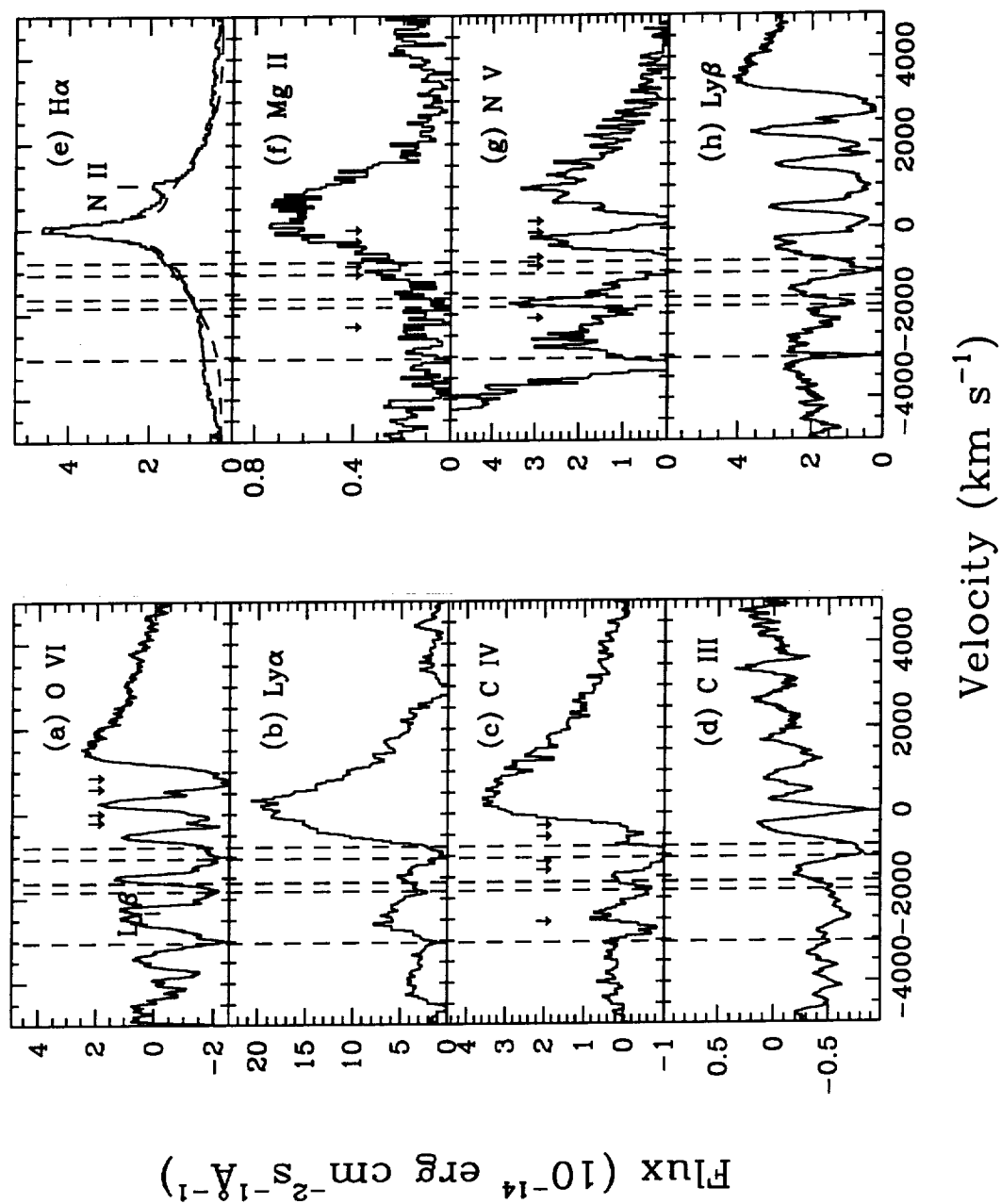
Fig. 1.—

Fig. 2.—

Fig. 3.—

Fig. 4.—

Fig. 5.—